

Energy & Environmental Science

Accepted Manuscript



This is an *Accepted Manuscript*, which has been through the Royal Society of Chemistry peer review process and has been accepted for publication.

Accepted Manuscripts are published online shortly after acceptance, before technical editing, formatting and proof reading. Using this free service, authors can make their results available to the community, in citable form, before we publish the edited article. We will replace this *Accepted Manuscript* with the edited and formatted *Advance Article* as soon as it is available.

You can find more information about *Accepted Manuscripts* in the [Information for Authors](#).

Please note that technical editing may introduce minor changes to the text and/or graphics, which may alter content. The journal's standard [Terms & Conditions](#) and the [Ethical guidelines](#) still apply. In no event shall the Royal Society of Chemistry be held responsible for any errors or omissions in this *Accepted Manuscript* or any consequences arising from the use of any information it contains.

Flexible Organic Tandem Solar Modules with 6% efficiency: Combining Roll-to-Roll Compatible Processing with High Geometric Fill Factors

G. D. Spyropoulos,^a P.Kubis,^{ac} N. Li,^a D. Baran,^a L. Lucera,^c M. Salvador,^a T. Ameri,^a M. M. Voigt,^{ab} F. C. Krebs^d and C. J. Brabec^{ab}

G. D. Spyropoulos, P.Kubis, N. Li, , D. Baran, Dr. M. Salvador, Dr. T. Ameri, Dr. M. M. Voigt, Prof. C. J. Brabec

^a Institute of Materials for Electronics and Energy Technology (i-MEET), Friedrich-Alexander-University Erlangen-Nuremberg, Martensstraße 7, 91058 Erlangen, Germany

L. Lucera, Dr. M. M. Voigt, Prof. C. J. Brabec

^b Bavarian Center for Applied Energy Research (ZAE Bayern), Haberstraße 2a, 91058 Erlangen, Germany

P.Kubis

^c Erlangen Graduate School in Advanced Optical Technologies (SAOT), Paul-Gordan-Str. 6, 91052 Erlangen, Germany

Prof. F. C. Krebs

^d Department of Energy Conversion and Storage, Technical University of Denmark, Frederiksborgvej 399, DK-4000 Roskilde, Denmark

Keywords: ((organic tandem solar cells, organic solar modules , solution-processing, laser patterning, flexible solar cells))

Abstract

Organic solar cell technology bears the potential for high photovoltaic performance combined with truly low-cost, high-volume processing. Here we demonstrate organic tandem solar modules on flexible substrates fabricated by fully roll-to-roll compatible processing at temperatures <70 °C. By using ultrafast laser patterning we considerably reduce the “dead area” of the modules and achieve geometric fill factors beyond 90%. The modules reveal very low interconnection-resistance compared to the single tandem cells and exhibit a power conversion efficiency of up to 5.7%. Bending tests performed on the modules suggest high mechanical resilience for this type of devices. Our findings inform concrete steps towards high efficiency photovoltaic applications on curved, foldable and moving surfaces.

Broader Context

The pressing need for inexpensive carbon neutral energy sources requires innovative approaches. Organic photovoltaics offers unique opportunities since it uses carbon based semiconductors, which can be processed from solution and deposited on flexible plastic substrates using high throughput roll-to-roll technologies. This allows for envisioning low-cost, lightweight solar to energy conversion platforms that could find applications in, amongst others, apparel, smart labels, building and car integrated photovoltaics, and moving robots. While roll-to-roll coated organic solar cell modules have been demonstrated in the past, the efficiency of those devices have been rather low, typically not exceeding 2% power conversion efficiency. Here we fabricate and characterize a multicell series stack of organic photovoltaic cells (tandem solar cells) on plastic foil using fully roll-to-roll compatible coating techniques. The solar cells feature a wide spectral response across the solar spectrum. We adopt a concept based on ultra-fast laser patterning for dividing the tandem cells into tandem modules. This process enables both high geometrical fill factors and low electrical interconnection losses. As a result, we achieve an unprecedented power conversion efficiency of ~6% for this type of devices. Bending tests certify the potential of this type of solar cells for applications that require high mechanical resilience.

Introduction

The pace with which the efficiency of organic photovoltaic devices (OPVs) has been progressing within the last decade allows for envisioning a significant share of this technology in the future's energy mix, thereby alleviating the world's increasing energy demand in an environmentally responsible way.¹⁻³ Crucially, OPVs provide excellent form factors, good performance under indoor lighting conditions and potentially very low energy production costs using solution processable organic semiconductors.⁴⁻⁷ The combination of these characteristics makes OPVs ideally suited for targeting niche markets that are incompatible with brittle semiconductors, e.g., off-grid portable charging, electronics in apparel and smart labels, as well as building and car integrated photovoltaics for non-planar surfaces,^{8,9} while simultaneously enabling production scale-up through roll-to-roll device fabrication.

Despite the recognized potential for high-throughput manufacturing, basic science limitations that have been preventing this technology from market implementation need to be addressed. Particularly, a poor match of the absorption spectrum of the active blend materials with the solar spectrum limits the photon harvesting capabilities and, consequently, the photocurrent generation. Additionally, thermalization losses diminish possible voltage outputs.^{10,11} One promising approach for overcoming these limitations is the tandem concept:^{12,13} sub-cells of different band-gap donor materials are typically combined in series for better matching the absorption of the device to the solar spectrum, while reducing the thermalization losses of the high-energy photons.¹⁴

The realization of hetero-tandem junction solar cells imposes several challenges from a material and device fabrication point of view. In addition to the requirement for complementary absorption of the absorber materials, the intermediate layer represents a critical link for achieving efficient optical and electrical coupling between the sub-cells, but also provides protection of the underlying layer against solvents from subsequently processed layers.¹⁵ Furthermore, photocurrent matching between the sub-cells is required, which can be controlled through the thickness of the active layers of the sub-cells and supported via the interlayer, which can provide recombination sites for better charge balance.^{16,17} While current champion organic tandem solar cells have been reported to deliver 10.6% power conversion efficiency (PCE) for solution-processed¹⁸ and 12% for vacuum processed (triple junction) devices (press release by Heliatek)¹⁹ these results still lack demonstration of the potential for high photovoltaic performance combined with truly low-cost, high-volume processing using roll-to-roll compatible techniques.

Although series connected tandem cells deliver open-circuit voltages as a result of the sum of the potentials of the sub-cells, the voltage typically falls short compared to the requirements as imposed by practical applications. A form of circumventing this limitation resides in the possibility of electrically interconnecting the solar cells into a photovoltaic module to further increase the voltage output. Ideally, PV modules should preserve the high PCE of individual cells while delivering high voltage outputs, which requires low ohmic losses and high geometric fill factors (GFF). The realization of an OPV module involves monolithic interconnection of consecutive cells. Typically, this interconnection is achieved with three patterning lines, providing electrical separation of the bottom electrode (P1), the active layer (P2) and the top electrode (P3), while the P2 line allows series connection between the top and bottom electrode of successive cells (**Figure 2a**).²⁰ The

greatest challenge in implementing an efficient module derives mainly from the tradeoff between the quality and the size of the interconnection area (dead area, **Figure 2a**). Although the dead area has no contribution to the photocurrent of the module, thus its size should be minimized, a sufficiently wide and defect-free P2 line is essential for ensuring low ohmic losses and, consequently, high module performance.²¹ The geometric fill factor is the ratio between the active and the total area of the module and determines the module efficiency for a specific size.

Several groups have tackled the problems involved in demonstrating efficient OPV module fabrication while aiming for facile processability using one and more-dimensional coating and/or printing technologies. For instance, Niggemann *et al.* presented 2% efficient single cell modules on glass (46.2 cm² active area) by utilizing photolithography or laser scribing for ITO structuring, a self-assembled monolayer (SAM) process for PEDOT:PSS patterning and mechanical scribing for active layer patterning.²² More recently, Etxebaria *et al.* introduced a solution processed roll-to-roll compatible patterning technology for the active layer based on an ink-jet printed SAM process (60 – 80% GFF).²³ This is a promising patterning technology as patterned lines with a width of 120 μm were demonstrated for inverted structure modules. One drawback could be the choice of SAM for guaranteeing chemical specificity towards the active layer and sufficient electrical interconnectivity. For demonstrating flexible OPV modules Kopola *et al.* used gravure printing, a 1-dimensional printing method which utilizes engraved cylinders.²⁴ Modules consisting of 5, 7 and 8 in series connected cells with power conversion efficiencies of 1.92%, 1.79% and 1.68%, respectively, were demonstrated based on ITO and evaporated metal back electrodes. One of the most technology relevant approaches for upscaling OPV modules on flexible substrates utilizing solution based roll-to-roll processing has been presented by the Krebs group.^{25 26 27 28 29} In these works, roll-to-roll coating methods based on slot-die coating and screen/flexo printing were used to produce monolithically, in series interconnected modules on ITO/polyethyleneterephthalat (PET), ITO/polyethyleneterephthalate (PEN) based substrates as well as ITO free substrates. Large area (360 cm²) modules suffered mainly from charge carrier extraction and performed at 1.7% while small area (4.8 cm²) modules produced an efficiency of 2.3% as the Ohmic losses were reduced.²⁵ The highest power conversion efficiency with this structure was 2.75% for a total active area of 35.5 cm².²⁷ Based on this progress on module fabrication, multilayer tandem polymer solar modules were demonstrated using roll-to-roll processing methods.^{30 31 32} The efficiency of these tandem modules was comparable to the efficiency of single junction modules (1.7% for 52.2 cm²), indicating the need for further material and method optimization, but doubtlessly demonstrating the feasibility of roll-to-roll printing for large-area OPV tandem production.

The approach developed in our research group aims at demonstrating high efficiency and virtually loss free OPV solar modules, when compared to the individual solar cells, with high GFF.²⁰ The concept was recently introduced by Kubis *et al.* who presented laser patterned OPV single junction modules based on ITO – metal (silver) – ITO (IMI) electrodes.³³ Here the serial interconnection between individual cells is accomplished with ultrafast depth-resolved laser patterning. This procedure takes advantage of the high spatial resolution intrinsic to laser scribing (typically in the μm range²⁰, as determined by the laser focal spot size of laser beam) as opposed to the limited, sub-mm resolution of most 1-D and 2-D coating techniques, where on site structuring of the OPV cells, e.g., through lateral displacement of the coating head, leads to rather

low GFFs.^{26 29 34} As a result, we demonstrated GFFs of over 90% for P3HT based modules on glass with over 3% PCE. For comparison, reported GFFs for modules realized *via* slot-die coating and screen printing are typically in the range of 70% or lower.^{35, 36} It is worth emphasizing the high roll-to-roll compatibility of our laser approach due to high processing speeds (up to 4 m/s).³³ Note that other groups have previously demonstrated practical examples of ultra-fast laser processing in combination with transparent, flexible electrodes.³⁷

In this report, we expand our concept toward high efficiency solution-processed flexible organic tandem solar modules by adopting fully roll-to-roll compatible processing. Individual organic tandem solar cells and tandem modules were fabricated under ambient conditions using solely commercially available materials and substrates. First, we fabricated flexible OPV tandem cells with PCE values of over 6% *via* doctor-blading. Doctor-blading is governed by similar working principles as slot die coating, and can be considered as an intermediate step between lab and mass production. Finally, 3-cell tandem modules with PCE values of 5.7% were produced by fs-laser patterning. On our final devices, we performed bending tests to demonstrate their flexibility and stability when considering future applications.

Experimental Section

Materials

OPV12¹⁷ (product no.: OPV12) was purchased from Polyera company. pDPP5T-2^{15, 17} (batch no.: GKS1-001) was provided by BASF. ZnO-nanoparticles dispersion in ethanol were received by Nanograde and used as a bottom buffer layer. ZnO-nanoparticle dispersion in acetone, used in the intermediate layer, was synthesized at the Technical University of Denmark (DTU)⁵. [60]PCBM (99.5 %) and [70]PCBM (99 %) were obtained from Solenne BV. Ba(OH)₂³⁸ and IMI-based flexible PET³³ were purchased from Sigma-Aldrich and Materion, respectively.

Tandem device fabrication

All photovoltaic devices were fabricated by doctor blading under ambient conditions with an inverted structure as shown in **Figure 1a**. Pre-patterned (P1 line) IMI-based PET foils (area of 11×16 cm²) were cleaned with isopropanol (IPA). After drying, the substrates were coated with a ≈30 nm thick ZnO layer and dried on a hot plate at 70 °C. A chlorobenzene based solution of OPV12: [60]PCBM (1:2 wt%, 32mg/ml in total) was coated on top to form ~150 nm bottom active layer. Subsequently, ~40 nm thick PEDOT HIL3.3 (1:5, diluted in IPA) and ~30 nm thick ZnO layer were bladed and dried at 70 °C for 5 min in air. We modified the ZnO layer by coating a ≈10 nm Ba(OH)₂ film on top (7 mg/ml in 2-methoxyethanol). Afterwards, we coated an 80 nm thick layer of pDPP5T-2:[70]PCBM (1:2 wt.% on top of the Ba(OH)₂), dissolved in a mixed solvent of 90% chloroform and 10% dichlorobenzene at a total concentration of 24 mg/ml) as the top active layer. As a final step, a 10 nm MoOx layer and 100 nm Ag layer were evaporated to form the top electrode.

Tandem module fabrication

The laser patterning was done with a LS - 7xxP laser patterning setup built by LS Laser Systems (München, Germany), consisting of the ultrafast laser femtoREGENTM UC - 1040 - 8000 fs Yb SHG from High Q Laser (Rankweil, Austria)³⁹ and the beam guiding system (4 mirrors and galvanometer scanner). The scanner's objective has a focal length of 330 mm and a focal spot diameter of $32 \pm 2 \mu\text{m}$ (at $1 / e^2$ intensity). The alignment of the laser beam was realized with the camera and the software positioning system developed by LS Laser Systems. The power of the laser was measured with the VEGA DISPLAY and 30A-BB-SH-18 ROHS sensor from Ophir Optronics (Jerusalem, Israel). The P1 line in the IMI was done with a laser fluence of 0.25 J/cm^2 and 50 % overlap. The P2 line in the tandem stack was done with a laser fluence of 0.085 J/cm^2 and an overlap of 94 %. The tandem layer consists of a stack of several single layers. In order to properly ablate all the material the laser passed the same line 3 times. In the last laser step evaporated Ag layer was removed with a laser fluence of 1.25 J/cm^2 and 66.6 % overlap. All lines were done with 520 nm wavelength.

Characterization

The area of the OSCs investigated in this work was defined by the top electrode, which was thermally evaporated through a mask with an opening of 10.4 mm^2 . After the deposition of top electrode, PET-based tandem solar cells were divided into smaller pieces (area of $2.5 \times 2.5 \text{ cm}^2$) to facilitate measurement. The $J-V$ characteristics were measured using a source measurement unit from BoTest. Illumination was provided by a solar simulator (Oriol Sol 1A, from Newport) with AM1.5G spectrum at 100 mW/cm^2 . Bending tests were performed by bending the devices on a drum with a diameter of 28 mm. Optical investigations of the thin films were carried out using an UV-VIS-NIR spectrometer (Lambda 950, from Perkin). EQE measurements were carried out using a QE-R system from Enlitech.

Results and discussion

A robust and efficient IMI coated PET foil ($7.7 \Omega/\text{sq}$) with superior electrical and mechanical (less brittleness) properties than ITO/PET substrates (in the order of $45 \Omega/\text{sq}$) was chosen as transparent bottom electrode for our tandem solar cells.^{33, 17} The complete architecture of our flexible tandem device is illustrated in **Figure 1a**. Briefly, a pre-patterned IMI based PET substrate was consecutively coated in air at temperatures lower than $70 \text{ }^\circ\text{C}$. As the active layer of the bottom sub-cell, we used a medium band gap conjugated polymer OPV12¹⁷ (obtained from Polyera) blended with the fullerene [60]PCBM. The top sub-cell was based on a blend consisting of the low bandgap co-polymer diketopyrrolopyrrole-quinuethiophene pDPP5T-2¹⁵ (BASF, batch no.: GKS1-001) and [70]PCBM. **Figure 1b** shows the UV-Vis spectra of the semiconducting polymers. The optical band gaps for OPV12 and pDPP5T-2 are 1.76 and 1.41 eV respectively, obtained from absorption measurements (see **Figure 1b**).¹⁷ As intermediate layer, we used PEDOT and ZnO layers with a total thickness of $\sim 60\text{-}80 \text{ nm}$. The ZnO surface was further modified with a thin, electron selecting $\text{Ba}(\text{OH})_2$ layer.^{38, 40} Finally, a molybdenum oxide layer (MoOx) and a Ag electrode were thermally evaporated. Alternatively, we are currently exploring solution

processable top electrodes, including semitransparent silver nanowires and colloidal Ag paint as possible candidates for replacing both ITO and thermally evaporated Ag.⁴¹⁻⁴³ Tandem cells prepared as described above delivered a record PCE of 6.12% with a V_{oc} of 1.35 V, which indicates an efficient and robust intermediate layer (**Figure 1c**, **Table S1**). A comparison of the $J-V$ characteristics between tandem cells and the corresponding single sub-cell is demonstrated in **Figure 1c**. The relatively high J_{sc} in the tandem cells is attributed to the efficient current matching between the bottom and top sub cells, which is supported by the EQE spectra (**Figure 1d**).

Next, we fabricated flexible tandem modules by interconnecting 3 single tandem solar cells in series. The interconnection procedure consists of laser ablation of the three patterning lines P1 – P3 (**Figure 2a**).⁴⁴ Selective laser ablation of the patterning lines is possible through precise adjustment of the laser fluence and overlap. First, the P1 line is scribed into the bottom 90 nm thick IMI layer without damaging the PET substrate to electrically isolate the three cells. Then, after depositing the active, intermediate and buffer layers the P2 interconnection line is patterned into the structure. Achieving a clean P2 line represents the key challenge of the laser patterning procedure for our tandem OPV modules. In this step, up to six organic and inorganic layers need to be ablated by the laser, without destroying or reducing the functionality of the bottom electrode and without creating substantial amounts of protrusion around the patterning line (see **Figure S3**). Finally, after thermal evaporation, the silver electrode was laser structured, without negatively affecting the subjacent layers, to form the P3 line and conclude the electrical interconnection of the tandem cells. The architecture of the whole module is schematically depicted in **Figure 2a**.

The dead area of the cell, which directly affects the GFF, is intrinsically related to the resolution of the patterning. We optimized the lateral width of the laser-ablation line P2, so that efficient interconnection between the rather thick tandem cells was possible while minimizing the dead area of the module. This requires a z-axis resolution in the nanometer regime and an x-y resolution in the micrometer scale. Both can be accomplished with ultrafast laser patterning, as proven by SEM (**Figure S3**, **S4**), optical imaging (**Figure 2b**) as well as $J-V$ characterization (**Figure 3a**).

The IMI foil was pre-patterned to accommodate nine substrates (**Figure S1**). Each substrate contained two reference single tandem cells and four tandem modules for best possible direct comparison. **Figure 2b**) shows a photograph of one of the substrates and optical microscope images capturing the P1 – P3 lines. The GFF was derived by calculating the ratio of the photoactive area and the total area (sum of the active and dead areas) (see **Figure S2**), neglecting possible bus bar losses. The $J-V$ performance of a representative reference tandem cell and the corresponding tandem modules are shown in **Figure 3a**. Additionally, **Table 1** summarizes the mean and best photovoltaic parameters.

In order to relate possible device losses in the module to the limitations given by the laser patterning processing, we varied the width of the P2 line (**Figure 2b**). We fabricated tandem modules with a narrow P2 line of $\approx 25 \mu\text{m}$ (Device B) and with a wide P2 line of $\approx 325 \mu\text{m}$ (Device C, see **Table 1**). In both cases, the P2 line is fully functional and the devices exhibit similarly high interconnection quality, as documented by the $J-V$ performance (**Figure 3a**). As a result, we were able to fabricate tandem modules with a champion efficiency of 5.70% (Device B). Device B with the narrower P2 line performed slightly better due to the smaller dead area, demonstrating the benefit of a laser controlled patterning approach. Remarkably,

the loss in PCE was below 7% compared to the reference tandem cell (Device A) and is mainly determined by losses in J_{sc} . The highest J_{sc} value (2.25 mA/cm²) is \approx 11% lower than the value corresponding to 1/3 of the reference cell, which represents the maximum limit for an in series connected module. Furthermore, V_{oc} values for the tandem module in the order of 3.90 V represent small voltage losses in the range of 3% compared with the combined total voltage given by three reference tandem cells. Moreover, encouraging FFs of 65% and 64% were observed in the case of device B and C, respectively. The increase in FF when compared to the reference tandem cell can be most likely attributed to smaller sub-area partitioning in the case of the modules. We highlight that by reducing the width of the P2 line from 325 μ m to 25 μ m in Device B the GFF of the module was significantly increased from 80% to 94% without affecting the interconnection quality, resulting in improved short-circuit current (2.25 mA/cm²).

From the dark J - V characteristic (inset of **Figure 3a**), we extracted the series resistance (R_s) and shunt resistance (R_{sh}) of our devices (**Table 1**). Comparison of the 3-cell modules with the single tandem devices reveals that the average R_s value for each sub-cell is almost the same as the R_s value of the reference device. This indicates that the interconnections generated by laser-patterning do not lead to additional ohmic losses. In addition, the laser patterning does not deteriorate the shunt resistance of the modules compared to the reference tandem device.

Previously, Kubis et al. demonstrated P2 lines in the range of 25 μ m for OPV single cell modules.³³ In a module the tandem configuration in series typically generates more voltage and less current, therefore the requirements on the current capacity of the P2 line are in part alleviated. However, precise control over the patterning of a multi-stack device is decisive for a successful integration of laser scribing into up-scaling technologies such as roll-to-roll coating.

Although flexible OPV single cells on IMI substrates have been demonstrated before,³³ the increased thickness of the tandem structure imposes additional strain on the devices. Tandem modules are particularly susceptible to device failure under mechanical stress, which can lead, amongst others, to delamination of the interconnection lines/areas and the recombination layer. Therefore, bending tests of flexible tandem modules are of utmost significance. **Figure 3b** depicts the normalized change in photovoltaic performance throughout 5000 bending cycles (drum radius 28 mm) for our tandem modules. Interestingly, we observed high mechanical resilience with a loss in PCE in the order of 2-7% that can be mainly attributed to losses in V_{oc} and J_{sc} . This suggests that the main cause is likely to be related to damage imposed on the charge-selecting and/or collecting layers and interfaces.

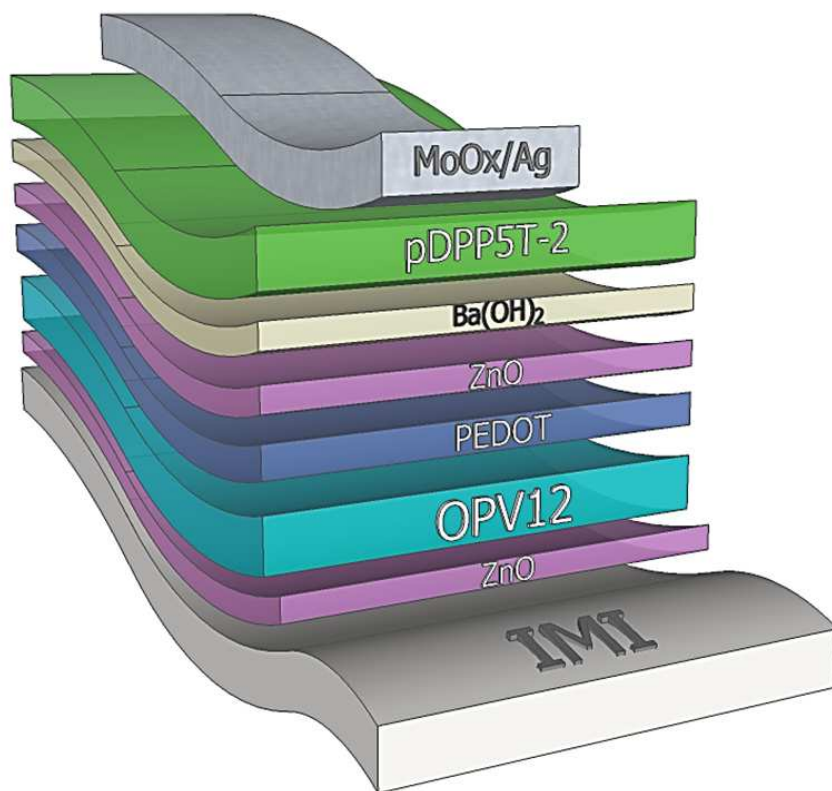
Conclusion

In summary, we demonstrate that high efficiency and reliable organic tandem modules can be processed on flexible substrates using a fs-laser as a means for separating and interconnecting the cells. The laser features high speed and high precision patterning in lateral and in z-directions. As a result, tandem modules with geometric fill factors beyond 90% and high-quality electrical interconnects are feasible, leading to minor photovoltaic losses compared to the non-patterned tandem cells. Considering the low temperatures involved (<70 °C) throughout device fabrication and possible laser writing speeds,

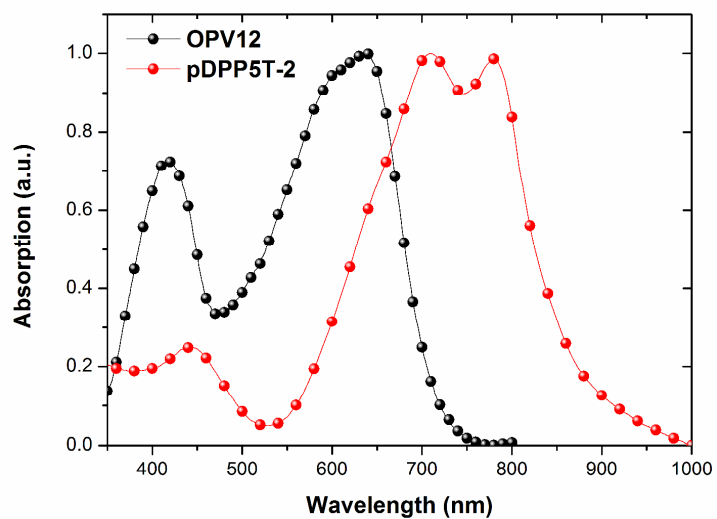
the process can be considered fully roll-to-roll, large scale compatible. Our champion tandem modules, consisting of three series connected cells, deliver a power conversion efficiency of 5.7% and a voltage output of 3.9 V. Bending tests manifest high mechanical resilience, demonstrating that this type of flexible cells could potentially be implemented as a power source on non-planar, foldable and movable surfaces of textiles, mechatronics and buildings.

Acknowledgements

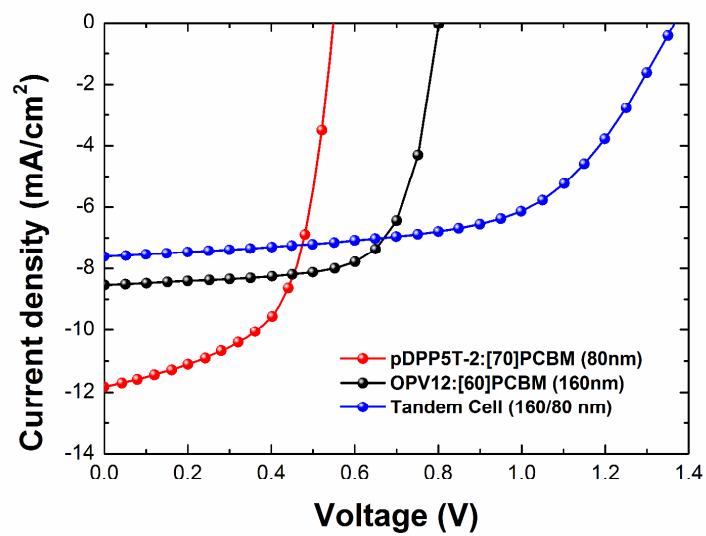
The authors thank Heraeus for providing PEDOT HIL 3.3. This work was financially supported by the European Commission as part of the Framework 7 ICT 2009 collaborative project ROTROT (“roll to roll production of organic tandem cells”, Grant no. 288565). The authors gratefully acknowledge the support of the Cluster of Excellence “Engineering of Advanced Materials (EAM)” at the University of Erlangen-Nuremberg, which is funded by the German Research Foundation (DFG) within the framework of its “Excellence Initiative”. The authors thank the support from Energy Campus Nuremberg (EnCN, Solarfactory), “Synthetic Carbon Allotropes” (DFG, SFB 953) project and “Solar Technologies Go Hybrid” (SolTech) project. D. Baran acknowledges Bavarian Research Foundation (BFS) for financial support. M. S. acknowledges primary support from a fellowship by the Portuguese Fundação para a Ciência e a Tecnologia (SFRH/BPD/71816/2010). The authors thank E. Epelbaum for performing SEM imaging.



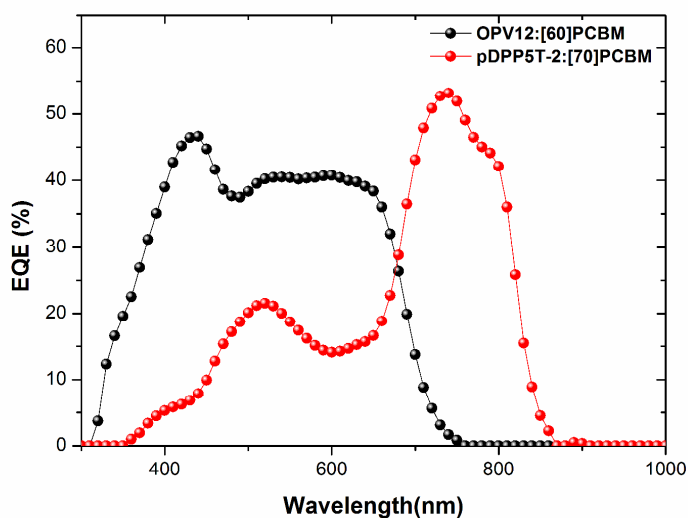
(a)



(b)

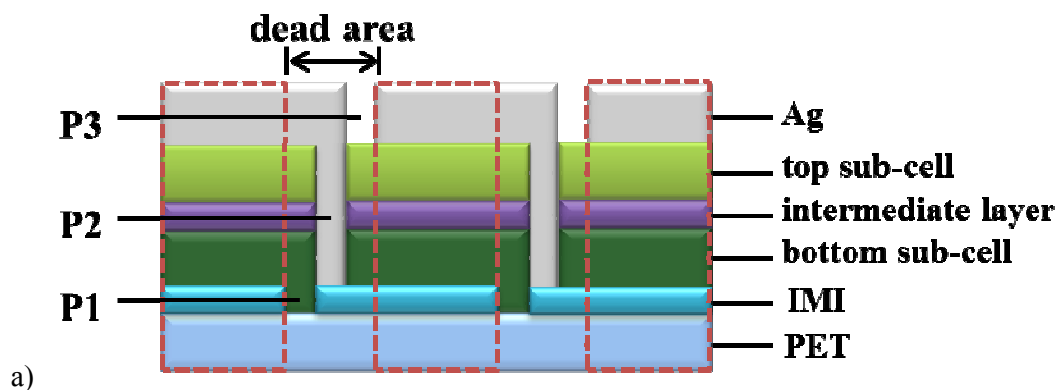


(c)

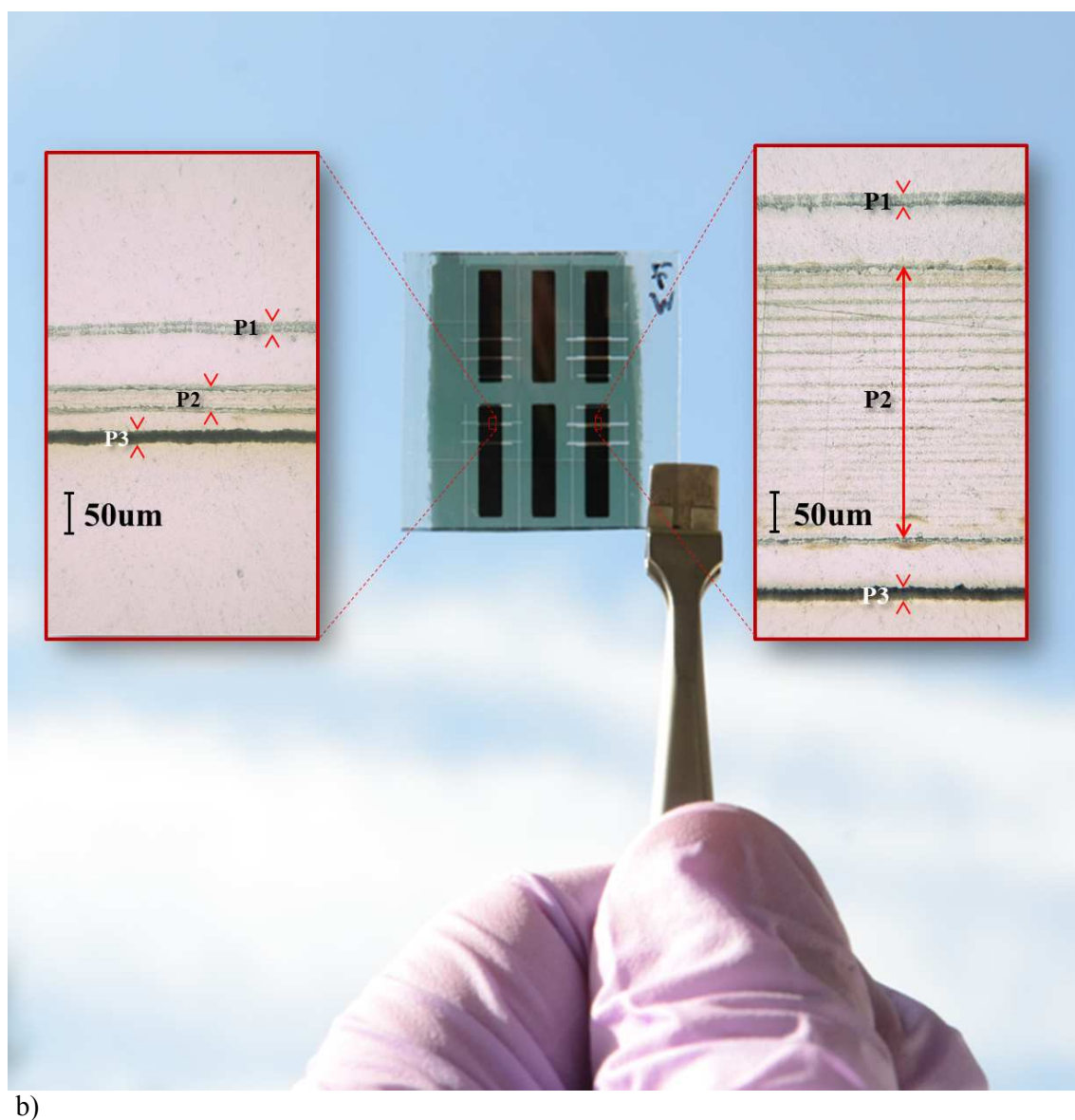


(d)

Figure 1. a) Schematic illustration of flexible tandem solar cell architecture. b) Absorption spectra of single OPV12:[60]PCBM and pDPP5T-2:[70]PCBM sub-cells. c) J-V characteristics of the OPV12, pDPP5T-2 based single cells and the corresponding tandem cell under illumination with an AM1.5G solar simulator and 100 mW/cm^2 . All devices were made on flexible substrates and processed in air. d) EQE spectra of single sub-cells. 750 nm light bias was used to obtain the EQE spectrum of the OPV12:[60]PCBM sub-cell while 550 nm light bias was used for the pDPP5T-2:[70]PCBM sub-cell.

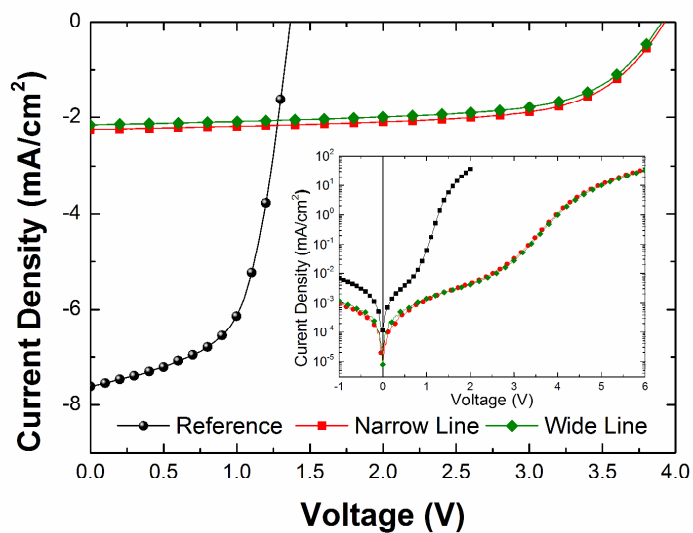


a)

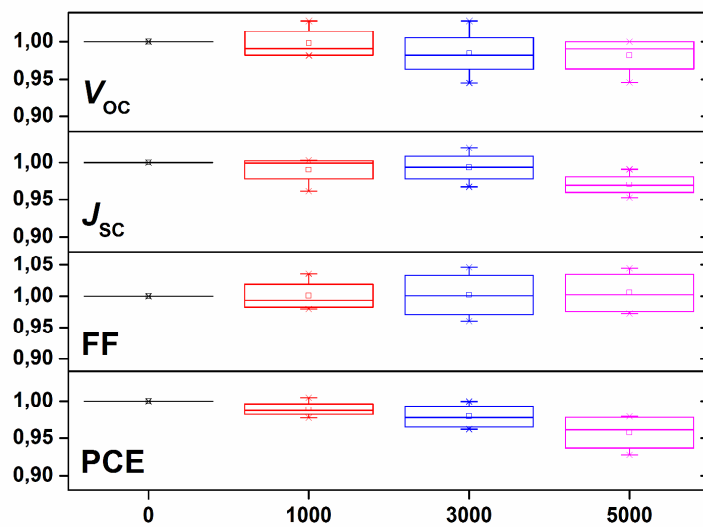


b)

Figure 2. a) Schematic illustration of the interconnection lines in the organic tandem module (3-cells module). b) Photograph of one of the 9 substrates carrying two reference single tandem cells (center) and two pairs of tandem modules (left and right), with narrow ($\approx 25 \mu\text{m}$, left) and wide ($\approx 325 \mu\text{m}$, right) P2 line patterning. The insets represent top views from an optical microscope displaying the lines P1 – P3. The wide P2 line was realized by laser hatching (scanning many single lines parallel to each other). As such, due to Gaussian energy distribution of the laser beam, rests of the absorber material are visible in the overlapping regions (lines visible in the P2 trench). This process did not affect the electrical interconnection quality of the P2 line.



(a)



(b)

Figure 3. a) J-V characteristics of reference tandem cells (black spheres) and tandem modules with narrow ($\approx 25 \mu\text{m}$, red squares) and wide ($\approx 325 \mu\text{m}$, green diamonds) P2 line under illumination. In inset shows the J-V characteristics in the dark.

b) Normalized device characteristics of flexible tandem module after 1000, 3000 and 5000 bending cycles.

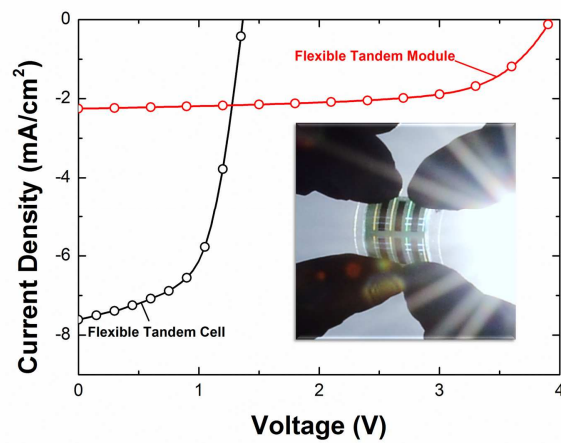
Table 1. Device parameters for OPV12/ pDPP5T-2 reference tandem cells (Device A) and tandem modules (Device B and C)

	V_{oc} (V)	J_{sc} (mA/cm ²)	FF (%)	PCE (%)	R_s (Ω cm ²)	R_{sh} (K Ω cm ²)	Device Area (mm ²)
Device A	1.35 (1.32 ^a)	7.61 (7.20 ^a)	60 (59 ^a)	6.12 (5.65 ^a)	10	160	10.4
Device B (\approx 25 μ m P2 line module)	3.92 (3.90 ^a)	2.25 (2.18 ^a)	65 (60 ^a)	5.70 (5.10 ^a)	30	1181	10.0
Device C (\approx 325 μ m P2 line module)	3.90	2.15	64	5.38	32	813	10.0

^aMean values of photovoltaic parameters were extracted from Figures S5.

Text

Flexible organic tandem solar modules with high geometric fill factors were constructed by utilizing a fully roll-to-roll compatible processing.

Graphic

1. Z. He, C. Zhong, S. Su, M. Xu, H. Wu and Y. Cao, *Nat. Photonics*, 2012, **6**, 591-595.
2. C. E. Small, S. Chen, J. Subbiah, C. M. Amb, S. W. Tsang, T. H. Lai, J. R. Reynolds and F. So, *Nat. Photonics*, 2012, **6**, 115-120.
3. M. A. Green, K. Emery, Y. Hishikawa, W. Warta and E. D. Dunlop, *Progress in Photovoltaics: Research and Applications*, 2013, **21**, 1-11.
4. C. J. Brabec, *Sol. Energy Mater. Sol. Cells*, 2004, **83**, 273-292.
5. F. C. Krebs, *Org. Electron.*, 2009, **10**, 761-768.
6. C. J. Brabec, S. Gowrisanker, J. J. M. Halls, D. Laird, S. Jia and S. P. Williams, *Adv. Mater.*, 2010, **22**, 3839-3856.
7. S. A. Gevorgyan, A. J. Medford, E. Bundgaard, S. B. Sapkota, H.-F. Schleiermacher, B. Zimmermann, U. Würfel, A. Chafiq, M. Lira-Cantu, T. Swonke, M. Wagner, C. J. Brabec, O. Haillant, E. Voroshazi, T. Aernouts, R. Steim, J. A. Hauch, A. Elschner, M. Pannone, M. Xiao, A. Langzettel, D. Laird, M. T. Lloyd, T. Rath, E. Maier, G. Trimmel, M. Hermenau, T. Menke, K. Leo, R. Rösch, M. Seeland, H. Hoppe, T. J. Nagle, K. B. Burke, C. J. Fell, D. Vak, T. B. Singh, S. E. Watkins, Y. Galagan, A. Manor, E. A. Katz, T. Kim, K. Kim, P. M. Sommeling, W. J. H. Verhees, S. C. Veenstra, M. Riede, M. Greyson Christoforo, T. Currier, V. Shrotriya, G. Schwartz and F. C. Krebs, *Sol. Energy Mater. Sol. Cells*, 2011, **95**, 1398-1416.
8. D. J. Lipomi, B. C. K. Tee, M. Vosgueritchian and Z. Bao, *Adv. Mater.*, 2011, **23**, 1771-1775.
9. M. Kaltenbrunner, M. S. White, E. D. Glowacki, T. Sekitani, T. Someya, N. S. Sariciftci and S. Bauer, *Nat. Commun.*, 2012, **3**.
10. R. A. J. Janssen and J. Nelson, *Adv. Mater.*, 2013, **25**, 1847-1858.
11. T. Kirchartz, K. Taretto and U. Rau, *J. Phys. Chem. C*, 2009, **113**, 17958-17966.
12. T. Ameri, G. Dennler, C. Lungenschmied and C. J. Brabec, *Energy Environ. Sci*, 2009, **2**, 347-363.
13. T. Ameri, N. Li and C. J. Brabec, *Energy Environ. Sci*, 2013, **6**, 2390-2413.
14. A. Hadipour, B. de Boer and P. W. M. Blom, *Adv. Funct. Mater.*, 2008, **18**, 169-181.
15. N. Li, D. Baran, K. Forberich, M. Turbiez, T. Ameri, F. C. Krebs and C. J. Brabec, *Adv. Energy Mater.*, 2013, **3**, 1597-1605.
16. A. Hadipour, B. de Boer, J. Wildeman, F. B. Kooistra, J. C. Hummelen, M. G. R. Turbiez, M. M. Wienk, R. A. J. Janssen and P. W. M. Blom, *Adv. Funct. Mater.*, 2006, **16**, 1897-1903.
17. N. Li, D. Baran, K. Forberich, F. Machui, T. Ameri, M. Turbiez, M. Carrasco-Orozco, M. Drees, A. Facchetti, F. C. Krebs and C. J. Brabec, *Energy Environ. Sci.*, 2013, **6**, 3407-3413.
18. J. You, L. Dou, K. Yoshimura, T. Kato, K. Ohya, T. Moriarty, K. Emery, C. C. Chen, J. Gao, G. Li and Y. Yang, *Nat. Commun.*, 2013, **4**.
19. *Heliatek consolidates its technology leadership by establishing a new world record for organic solar technology with a cell efficiency of 12%*, Heliatek GmbH, 2013.
20. P. Kubis, N. Li, T. Stubhan, F. Machui, G. J. Matt, M. M. Voigt and C. J. Brabec, *Progress in Photovoltaics: Research and Applications*, 2013, n/a-n/a.
21. H. Hoppe, M. Seeland and B. Muhsin, *Sol. Energy Mater. Sol. Cells*, 2012, **97**, 119-126.
22. M. Niggemann, B. Zimmermann, J. Haschke, M. Glatthaar and A. Gombert, *Thin Solid Films*, 2008, **516**, 7181-7187.
23. I. Etxebarria, J. G. Tait, R. Gehlhaar, R. Pacios and D. Cheyngs, *Org. Electron.*, 2013, **14**, 430-435.
24. P. Kopola, T. Aernouts, R. Sliz, S. Guillerez, M. Ylikunnari, D. Cheyngs, M. Välimäki, M. Tuomikoski, J. Hast, G. Jabbour, R. Myllylä and A. Maaninen, *Sol. Energy Mater. Sol. Cells*, 2011, **95**, 1344-1347.
25. F. C. Krebs, S. A. Gevorgyan and J. Alstrup, *J. Mater. Chem.*, 2009, **19**, 5442-5451.
26. F. C. Krebs, T. Tromholt and M. Jørgensen, *Nanoscale*, 2010, **2**, 873-886.
27. F. C. Krebs, J. Fyenbo and M. Jørgensen, *J. Mater. Chem.*, 2010, **20**, 8994-9001.
28. F. C. Krebs, *Sol. Energy Mater. Sol. Cells*, 2009, **93**, 1636-1641.
29. F. C. Krebs, *Organic Electronics: physics, materials, applications*, 2009, **10**, 761-768.
30. T. R. Andersen, H. F. Dam, B. Andreasen, M. Hösel, M. V. Madsen, S. A. Gevorgyan, R. R. Søndergaard, M. Jørgensen and F. C. Krebs, *Sol. Energy Mater. Sol. Cells*, 2014, **120, Part B**, 735-743.
31. F. Livi, R. R. Søndergaard, T. R. Andersen, B. Roth, S. Gevorgyan, G. D. Spyropoulos, J. Adams, T. Ameri, C. J. Brabec, M. Legros, N. Lemaître, S. Berny, S. Schumann, P. Apil, M. Vilkmann, F. C. Krebs, **Submitted 2014**.
32. T. R. Andersen, H. F. Dam, M. Hoesel, M. Helgesen, J. E. Carle, T. T. Larsen-Olsen, S. A. Gevorgyan, J. W. Andreasen, J. Adams, N. Li, F. Machui, G. D. Spyropoulos, T. Ameri, N. Lemaître, M. Legros, A. Scheel, D. Gaiser, K. Kreul, S. Berny, O. R. Lozman, S. Nordman, M. Valimaki, M. Vilkmann, R. R. Søndergaard, M. Jørgensen, C. J. Brabec and F. C. Krebs, *Energy Environ. Sci.*, 2014.
33. P. Kubis, L. Lucera, F. Machui, G. D. Spyropoulos, J. Cordero, A. Frey, J. Kaschta, M. M. Voigt, G. J. Matt, E. Zeira, C. J. Brabec, **Accepted 2014**, DOI:10.1016/j.orgel.2014.06.006.
34. F. C. Krebs, J. Fyenbo, D. M. Tanenbaum, S. A. Gevorgyan, R. Andriessen, B. Van Remoortere, Y. Galagan and M. Jørgensen, *Energy Environ. Sci*, 2011, **4**, 4116-4123.
35. Press release, <http://www.konarka.com/> (May, 2012).
36. F. C. Krebs, *Sol. Energy Mater. Sol. Cells*, 2009, **93**, 394-412.
37. E. Kymakis, K. Savva, M. M. Stylianakis, C. Fotakis and E. Stratakis, *Adv. Funct. Mater.*, 2013, **23**, 2742-2749.
38. H. Zhang, T. Stubhan, N. Li, M. Turbiez, G. J. Matt, T. Ameri and C. J. Brabec, **Submitted 2014**.
39. V. Matylytsky, P. Kubis, C. Brabec and J. A. der Au, High Q femtoREGENTM UC laser systems for industrial microprocessing applications, 2012.

40. N. Li, D. Baran, G. D. Spyropoulos, H. Zhang, S. Berny, M. Turbiez, T. Ameri, F. C. Krebs and C. J. Brabec, *Adv. Energy Mater.*, 2014, n/a-n/a.
41. K. F. J. Krantz, P. Kubis, F. Machui, J. Min, T. Stubhan and C. J. Brabec, 2014.
42. J. Krantz, T. Stubhan, M. Richter, S. Spallek, I. Litzov, G. J. Matt, E. Spiecker and C. J. Brabec, *Adv. Funct. Mater.*, 2013, **23**, 1711-1717.
43. F. Guo, X. Zhu, K. Forberich, J. Krantz, T. Stubhan, M. Salinas, M. Halik, S. Spallek, B. Butz, E. Spiecker, T. Ameri, N. Li, P. Kubis, D. M. Guldi, G. J. Matt and C. J. Brabec, *Adv. Energy Mater.*, 2013, **3**, 1062-1067.
44. N. Li, P. Kubis, K. Forberich, T. Ameri, F. C. Krebs and C. J. Brabec, *Sol. Energy Mater. Sol. Cells*, 2014, **120**, **Part B**, 701-708.